Moving Horizon Estimator Design for a Nanoparticle Synthesis Batch Process ⋆

Marcel Kévin Jiokeng Dongmo * **Yang Guohui** **
Hermann Nirschl ** **Thomas Meurer** *

* Digital Process Engineering Group, MVM, Karlsruhe Institute of
Technology, Hertzstr. 16, 76187 Karlsruhe, Germany
(e-mail: {marcel.dongmo, thomas.meurer}@kit.edu).
** Process Machines Group, MVM, Karlsruhe Institute of Technology,
Straße am Forum 8, 76131 Karlsruhe, Germany
(e-mail: {guohui.yang, hermann.nirschl}@kit.edu).

Abstract: An approach for the real-time state estimation for particulate systems using an early-lumping moving horizon estimator is presented. The synthesis of particles is characterized by a complex system of partial differential equations and ordinary differential equations and optimization-based parameter identification techniques are employed to precisely determine process parameters. Subsequently, model order reduction through the dynamic mode decomposition with control is performed to obtain a linear approximation of the inherently nonlinear system while preserving critical dynamic features. The resulting system serves as the foundation for the moving horizon estimator design, which operates by solving a constrained optimization problem. This optimization problem is designed to minimize the discrepancy between measured and estimated outputs, thus providing accurate real-time state estimation. The applicability of the proposed approach is illustrated by investigating the synthesis of aluminum-doped zinc-oxide particles as a case study with the goal to reconstruct the particle size distribution based on the estimated concentration of the aluminum-doped zinc-oxide nanocrystals.

Keywords: Moving horizon estimation, particulate systems, dynamic mode decomposition, crystallization, model order reduction, population balance equation.

1. INTRODUCTION

While extensive research exists regarding the modeling and control of particulate systems, see, e.g., Stolzenburg and Garnweitner (2017); Wu and Yang (2019), the precise manipulation of particle and product properties, including critical factors such as particle size distribution (PSD), number concentration (NC), and fractal dimension, remains a formidable challenge. In response to this challenge, a moving horizon estimator (MHE), see, e.g., Rao et al. (2003); Kühl et al. (2011); Dongmo and Meurer (2022), is designed to dynamically determine particle properties in real-time.

Here, a time-resolved insights into the characteristics of particulate systems is proposed, where the focus is on modeling the intricate particle synthesis process, which inherently comprises a population balance equation (PBE) that is modeled by means of a partial differential equation (PDE), see, e.g., Falola et al. (2013); Kang et al. (2022) and the reaction kinetics of solutes in the solution is described by ordinary differential equations (ODEs), see, e.g., Ramkrishna (2000); Stolzenburg and Garnweitner (2017). The resulting PDE-ODE system is discretized and solved to obtain the PSD and the related moments of the

PBE. As a concrete illustration, this approach is employed to investigate the generation of aluminum-doped zinc-oxide (AZO) particles. This process involves the meticulous mixing of aluminum and zinc precursors within a non-aqueous solution under given reaction conditions in a batch reactor. The process in question has previously been examined in the studies Ungerer et al. (2019, 2020a). These investigations led to the establishment of a correlation between zinc precursor consumption and the growth of AZO nanocrystals. However, these analyses did not provide insights into the evolution of the PSD. In the current work, the primary objective is to leverage offline measurements of AZO mass and NC to reconstruct the PSD online. This reconstruction is achieved by utilizing the number density of the particles and making use of the moments of the PBE.

Recognizing the computational challenges posed by the inherently nonlinear nature of the system, various methods were developed to solve the PBE analytically, see, e.g., J. McCoy and Madras (2003) and by making use of the discrete population balance methods (Kumar and Ramkrishna, 1996). A model order reduction strategy is employed, namely, the dynamic mode decomposition with control (DMDc) (Proctor et al., 2016) to transform the complex, high-dimensional system into a simplified linear representation while preserving essential dynamic characteristics.

With the reduced-order model in hand, a MHE is developed, see, e.g., Dongmo and Meurer (2022), where MHE is applied on a PDE-ODE system with sensor dynamics. This estimator is designed to dynamically predict system behavior by minimizing the discrepancy between measured and estimated AZO concentration. The approach entails solving a constrained optimization problem, which optimally adjusts the estimated outputs in real-time, enhancing the ability to track and control the PSD effectively. A similar approach was studied in Li et al. (2023) in the context of large-scale nonlinear processes, however in the absence of first-principles process models.

The paper is organized as follows. In Section 2, an overview of the particle synthesis process is provided and relevant measurement techniques are introduced, which lay the foundation for understanding the particle growth process detailed in Section 3. Section 4 investigates the DMDc-based MHE technique, where a linear system is introduced to approximate the inherently nonlinear behavior of the PDE-ODE system. Simulation results are presented in Section 5, offering empirical insights into the practical application of our approach. Finally, in Section 6, findings are summarized and potential future directions and outlooks for this research are discussed.

2. PARTICLE SYNTHESIS AND METHODOLOGY

The synthesis of AZO nanocrystals in this study builds upon the prior research conducted in Ungerer et al. (2019). Herein, the synthesis of AZO nanocrystals follows the non-aqueous benzylamine route using specific crystalline precursors is employed: zinc acetylacetonate hydrate ($Zn(acac)_2$ powder, purity $\geq 99\%$, Aldrich) and aluminum isopropoxide ($Al(OiPr)_3$, purity $\geq 98\%$, Aldrich). These precursors are initially introduced into the reaction at a concentration of $C_E = 25g\ L^{-1}$, with the molar fraction of the aluminum precursor intentionally set at 2.5 mol%. As the reaction medium, the aromatic solvent benzylamine ($BnNH_2$, benzylamine for synthesis, purity $\geq 99\%$, Merck) is utilized.

The synthesis procedure is carried out in a closed reactor equipped with a glass inlet (volume: 350mL), as schematically illustrated in Fig. 1. The reaction temperature is maintained at 110°C under a total overpressure of 1 barg for a process simulation duration of $T_{sim} = 3h$. Initially, the sparingly soluble precursors were pre-dissolved within the reactor through continuous stirring at 50°C for 15 minutes. Subsequently, the reaction solution was rapidly heated to the process temperature at a rate of 6 K min^{-1}. Regular sampling is performed during the process with each sample having a volume of 10mL obtained through overpressure via a riser. Ethanol is then employed to dissolve the remaining precursor and lower the reaction temperature to the ambient value of 25°C.

The investigation of the AZO particle formation processes via the benzylamine route involves a comprehensive set of characterization techniques. To gain insights into key parameters such as the radius of gyration, fractal dimensions and PSD, a small-angle X-ray scattering (SAXS) camera is used, see, e.g., Goertz et al. (2012); Nirschl and Guo (2018). SAXS data analysis allows us to extract valuable information regarding the structural aspects of the AZO
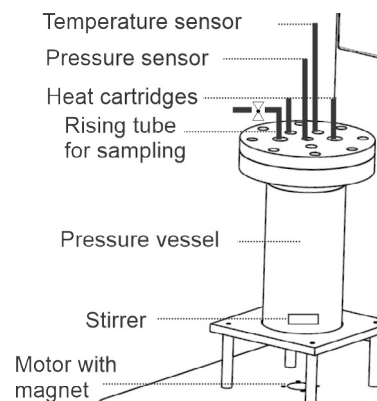

Fig. 1. Schematics of the batch reactor.

particles that are needed for the parameter identification of the PDE-ODE model.

For a time-resolved kinetic analysis of AZO nanocrystal growth during the synthesis, gravimetry analysis is employed. This technique provides crucial data on the evolution of particle mass over time, offering insights into the growth kinetics of the particles as shown in Fig. 2, where the normalized concentrations of both precursors and AZO particles are depicted. The kinetic model describing AZO crystals growth is obtained by utilizing the pseudo-first-order kinetic model, see, e.g., Garnweitner and Grote (2009) for similar kinetic behaviors.
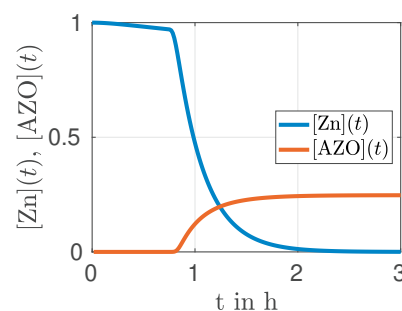

Fig. 2. Normalized concentrations of precursors and AZO particles.

To further characterize the size, shape, and crystal structure of AZO particles at various stages of growth during the synthesis, transmission electron microscopy (TEM) is utilized. In this process, samples are diluted with ethanol and air-dried on a TEM grid at 25°C. The mean size distribution of AZO particles is quantitatively assessed by analyzing a substantial population of particles, using specialized software such as ImageJ. This methodology facilitates a comprehensive investigation of particle morphology and crystal structure at various points throughout the synthesis process, as visually represented in Fig. 3. The examination reveals that the growth process of the spherical diameter, also referred to as the size of AZO nanocrystals, can be delineated into three distinct stages. In the initial stage of Fig. 3, the process begins with homogeneous nucleation within the first three minutes, followed by the uniform growth of nuclei. This ultimately results in the formation of single AZO primary nanocrystals characterized by their roughened surfaces. In the second stage, the primary AZO nanocrystals also call monocrystals undergo

exponential growth, following pseudo-first-order kinetics, until the entire zinc precursor is consumed. Due to the low concentration of the aluminum precursor compared to the zinc precursor, its involvement in the reaction process is neglected. In the absence of a stabilizer, this stage leads to an oriented aggregation of the primary crystals, resulting in the formation of hexagonal-shaped AZO mesocrystals characterized by internal grain boundaries. During the third phase, the growth of primary crystals concludes, allowing the subsequent processes of densification and orientation to take place.
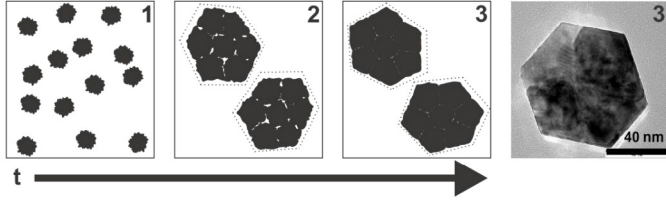

Fig. 3. Growth of AZO particles (Ungerer et al., 2019).

3. PROBLEM FORMULATION

3.1 Mathematical model

The particle synthesis process is modeled by considering both the reaction kinetics of the precursors and the PBE, which describes the evolution of the particle size distribution and particle number density over time as

$$\partial_t[Zn](t) = -k(T)[Zn](t), \quad t > 0$$
$$\partial_t n(x,t) = -G([Zn])\partial_x n(x,t) + B([Zn],x) - \quad (1a)$$
$$P_{agg}([Zn],x)n(x,t)$$

on $z \in (0, x_{max})$, $t > 0$ with boundary conditions

$$n(0,t) = 0, \qquad t > 0, \quad (1b)$$

and initial conditions

$$n(x,0) = n_0(x), \quad [Zn](0) = [Zn]_0, \quad x \in [0, x_{max}]. \quad (1c)$$

Herein, $[Zn]$ denotes the zinc precursor concentration, $n(x,t)$ the particle number density of monocrystals, and x the particle size. The PBE is composed of three main parts: the growth term $G([Zn])\partial_x n(x,t)$, the nucleation term $B([Zn],x)$ and the aggregation term $P_{agg}([Zn],x)n(x,t)$ defined as

$$B([Zn],x) = k_{nuc}k(T)[Zn]^b\phi(x,\mu_{mono}),$$
$$G([Zn]) = k_g k(T)[Zn]^g, \quad (2)$$
$$P_{agg}([Zn],x) = k_{agg}k(T)[Zn]^a P(x,\mu_{agg}),$$

where $\phi(x,\mu_{mono})$ denotes a normal distribution function with mean μ_{mono} and $P(x,\mu_{agg})$ is the probability that particles with size x aggregate at μ_{agg}. The model parameters $\boldsymbol{p} = [\mu_{mono}, \mu_{agg}, b, g, a, k_{nuc}]$ are identified subsequently based on measurement data from the real plant, with k_g and k_{agg} being set to 1. The rate constant $k(T)$ describes the temperature dependency of the underlying chemical reaction process, and it is modeled using the Arrhenius law, as introduced in Ungerer et al. (2020b). The output of the system is defined as

$$\partial_t \nu(x_m,t) = P_{agg}([Zn],x)n(x,t), \quad (3)$$

where $\nu(x_m,t)$ is the number density of generated mesocrystals with size $x_m \in [0, x_{max}]$. The AZO concentration of mesocrystals follows as

$$[AZO](t) = y(t) = \frac{M_{AZO}}{N_{avo}v_{AZO}}M_3(t), \quad (4)$$

see Perala and Kumar (2014), with N_{avo} the Avogadro number and M_{AZO} as well as v_{AZO} the molecular mass and unit volume of a AZO monocrystal, respectively. Here, $M_3(t)$ is the third moment of (3), which is given by

$$M_3(t) = \int_0^{x_{max}} x^3 \nu(x,t)dx. \quad (5)$$

The total particle number or NC is obtained by exploiting the zeroth moment of (3), which is given by

$$M_0(t) = N_{M_0}(t) = \int_0^{x_{max}} \nu(x,t)dx. \quad (6)$$

Based on the offline measurement data, [AZO], the NC and the PSD are determined and employed for the parameterization of the model. The temperature $T(t)$ in the reactor is assumed homogeneous and is introduced into the model using

$$\tau \partial_t T(t) = -T(t) + v, \quad (7)$$

where τ represents a time constant and v refers to the energy generated by heating cartridges. A secondary PI controller is implemented at the reactor so that in view of the comparatively (w.r.t. to the particle process) quick temperature response $T(t)$ can be considered as the control input. The particle synthesis occurs in two distinct steps: the preheating phase of the process is conducted at 50°C, while the synthesis phase is carried out at 110°C.

For the subsequent analysis, the PDE described in (1) is discretized in x using backward finite-differences.

3.2 Parameter identification

The model parameters $\boldsymbol{p}$ are all positive and determined through solving the optimization problem

$$\min_{\boldsymbol{p}} \sum_{i=1}^{N_t} \Big[\Big(N_{meas}(t_i) - \hat{N}_{M_0}(t_i)\Big)^2 + $$
$$\Big([AZO]_{meas}(t_i) - \hat{y}(t_i)\Big)^2 + \quad (8a)$$
$$\sum_{j=1}^{q}\Big(\nu(x_j,t_i) - \hat{\nu}(x_j,t_i)\Big)^2\Big]$$

subject to (1), (3) and (4), where $N_{meas}(t)$, $[AZO]_{meas}(t)$ and $\nu(x,t)$ represent the measured NC, AZO concentration and particle number density of mesocrystals, respectively. The optimization problem minimizes the discrepancy between data obtained from the actual plant and the predicted states and is carried out employing a SQP algorithm. The temperature profile of the synthesis process, along with the five collected samples, are illustrated in Fig. 4a-d. Here, the data encompass various parameters, including the PSD (black dashed lines), particle mass (red dots), and number concentration (red dots). The final data point for mass concentration, as illustrated in Fig. 4b exhibits a significant deviation from the preceding samples, which may be attributed to measurement errors.

The results of the parameter identification are shown in Fig. 4b-d. The depicted figures show a good agreement between the optimized model and the measured data, indicating a successful optimization process and a good fit of the data. The following parameter values were obtained: $\mu_{mono} = 23$nm, $\mu_{agg} = 58$nm, $b = 5.29$, $g = 9.19$, $a = 0.85$, $k_{nuc} = 10^{14.84}$ with the initial state set as $[Zn](0) = 25$

a) Temperature profile.
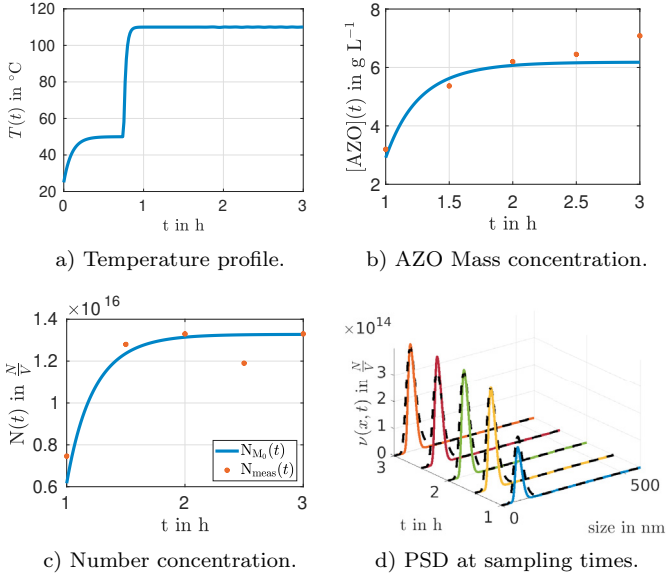
b) AZO Mass concentration.

c) Number concentration.

d) PSD at sampling times.

Fig. 4. Results of the data-based parameter identification.

g L^{-1}, $n_0(x) = 0$, where $x \in [0, 574]$nm, $t \in [0,3]$h and a spatial discretization with $q = 400$ intervals and $N_t = 200$ time discretization steps. The black dashed and the colored continuous lines in Fig. 4d represent the PSD measurements and the reconstructed PSD at sampling times, respectively. The identified model is subsequently used to extract the snapshots needed for the DMDc.

4. DMD AND MOVING HORIZON ESTIMATION

The objective of this section is to develop a moving horizon estimator based on the reduced-order model derived from the introduced PDE-ODE system.

4.1 Dynamic mode decomposition with control

The model order reduction is accomplished using DMDc, as detailed in Proctor et al. (2016). The primary objective is to identify a time-discrete linear approximation of (1a) based on measured data, aiming to achieve

$$\dot{X} = f(X, T, t) \qquad \rightarrow \qquad x_{i+1} = Ax_i + bT_i,$$

where $X(t) = \left[[Zn](t), n(x_j, t), \nu(x_j, t)\right]^T$, $b \in \mathbb{R}^{2q+1}$, $A \in \mathbb{R}^{2q+1 \times 2q+1}$, $x_i = \left[[Zn]_i, n_i, \nu_i\right]^T \in \mathbb{R}^{2q+1}$, $T_i \in \mathbb{R}$, $n_i \in \mathbb{R}^q$, $\nu_i \in \mathbb{R}^q$, $[Zn]_i \in \mathbb{R}$ for $i \in \{0, 1, ..., m\}$ and $j \in \{1, ..., q\}$. Here, i denotes the time discretization index and the simulation time interval is discretized in $m + 1$ stages. The reaction temperature at time i is given by T_i.

The essence of this approach lies in determining the matrice A and the vector b, effectively summarizing the primary dynamic traits of the system and optimizing their alignment with the available data. To achieve this, the process is initiated by parameterizing (1), (2) and (3). Subsequently, snapshots X_1, X_2 and Y are gathered from the parameterized model at regular time intervals $\Delta t = \frac{T_{\text{sim}}}{m}$, capturing state and input behavior in

$$\begin{aligned} X_1 &= [x(t_0)\, x(t_1) \dots x(t_{m-1})] \\ X_2 &= [x(t_1)\, x(t_2) \dots x(t_m)] \\ Y &= [T(t_0)\, T(t_1) \dots T(t_{m-1})] \end{aligned} \quad (9)$$

such that

$$X_2 \approx AX_1 + bY = [A\ b]\begin{bmatrix} X_1 \\ Y \end{bmatrix}, \quad X_2 \approx G\Omega, \quad (10)$$

where the optimal $G = [A\ b]$ is calculated by minimizing the residual in terms of Frobenius norm $\| X_2 - G\Omega \|_f$. This is achieved by performing the singular value decomposition (SVD) of the input subspace $\Omega = \left[\begin{smallmatrix} X_1 \\ Y \end{smallmatrix}\right]$ and by using the reduced left singular matrix $\tilde{U}$ to map the state in the original space

$$G = X_2\Omega^\dagger \quad \text{with} \quad \Omega = U\Sigma V^* \approx \tilde{U}\tilde{\Sigma}\tilde{V}^*$$

$$G \approx \bar{G} = X_2\tilde{V}\tilde{\Sigma}^{-1}\tilde{U}^* = X_2\tilde{V}\tilde{\Sigma}^{-1}[\tilde{U}_1^*\ \tilde{U}_2^*] \quad (11)$$

$$[A\ b] \approx [\bar{A}\ \bar{b}] = [X_2\tilde{V}\tilde{\Sigma}^{-1}\tilde{U}_1^*,\ X_2\tilde{V}\tilde{\Sigma}^{-1}\tilde{U}_2^*].$$

Here $\tilde{U}_1 \in \mathbb{R}^{2q+1 \times p}$, $\tilde{U}_2 \in \mathbb{R}^{1 \times p}$, where p is the truncation order, $\bar{A} \in \mathbb{R}^{2q+1 \times 2q+1}$, $\bar{b} \in \mathbb{R}^{2q+1}$ and the mapping of the states for a low number of data points is obtained as

$$x_{i+1} = \bar{A}x_i + \bar{b}T_i, \quad (12)$$

which represents the full DMDc approximation obtained based on the truncation order p. The advantage of employing DMDc lies in the fact that it effectively accounts for both an accurate system behavior and a fast computation depending on the number of $m + 1$ time intervals. The system output, which represents the number density of mesocrystals is labeled as ν_i. It is a subset of x_i and admits a representation of the form

$$\nu_i = \bar{C}x_i, \quad (13)$$

with the output matrix $\bar{C} \in \mathbb{R}^{q \times 2q+1}$. The discrete AZO concentration can be rewritten as

$$[\text{AZO}]_i = y_i = \bar{c}^T\nu_i, \quad (14)$$

where $\bar{c}^T \in \mathbb{R}^{1 \times q}$ is a row vector composed of (4) and the discretized integral in (5). Note that this integral is implemented using the trapezoidal rule.

Remark 1. For a high number of discretization points, additional model reduction can be achieved by conducting the SVD on the output subspace $X_2 \approx \hat{U}\hat{\Sigma}\hat{V}^*$ with a much lower truncation degree r.

4.2 Moving horizon estimation

The primary objective of MHE is to minimize the quadratic error between measured and estimated values over a finite receding horizon θ. In this context, the focus is on reconstructing the PSD based on the parameterized system (1) under disturbances. To achieve this, the reduced-order model (12) is used to represent the system dynamics. Hereby, only the measured AZO concentration y_i is employed for the estimation process. Hence, the state estimation problem can be formulated as

$$\min_{\hat{x}_{k-\theta}} J = \frac{1}{2} \int \left(\Delta y(t)\right)^2 dt$$
$$\approx \frac{\Delta t}{4} \sum_{i=k-\theta}^{k-1} \left[(\Delta y_{i+1})^2 + (\Delta y_i)^2\right] \quad (15a)$$

for $\Delta y_i = y_i - \hat{y}_i$ subject to

$$\hat{x}_{i+1} = \bar{A}\hat{x}_i + \bar{b}T_i, \quad i = k - \theta, \dots, k - 1, \ k \in \mathbb{N}_{\geq 0} \quad (15b)$$

with $\theta \in \mathbb{N}_{>0}$ denoting the horizon length. The initial value $\hat{x}_{k-\theta}$ represents the decision variable and T_i corresponds to the temperature input at discrete time i, respectively. The function J is approximated by making use of the trapezoidal rule. The optimization problem (15) is solved

repeatedly on the receding finite time horizon θ to find the optimal initial state $\hat{\boldsymbol{x}}_{k-\theta}$ minimizing J.

5. SIMULATION RESULTS

The particle synthesis process extends over a total duration of three hours with the initial precursor concentration $C_E = 25$g L^{-1}. The initial 45 minutes of this time frame are dedicated to the preheating phase. During this phase, the solution's temperature is raised to $T_{R,\text{pre}} = 50$°C over a 30-minute period and is subsequently maintained at this level for additional 15 minutes. This temperature adjustment is made to ensure favorable solubility of the precursor species. Importantly, it is assumed that no particles are formed during this preheating phase due to the relatively low temperature.

Following the preheating phase, the synthesis phase commences, during which the solution's temperature is rapidly increased to the desired reaction temperature of 110°C. The first sample is collected as soon as the reaction temperature is reached, which occurs one hour after the start of the process. Subsequent samples are taken at regular intervals of 30 minutes to monitor the progress of the synthesis over time, as shown in Fig. 4. These data are employed for parameterizing the mathematical model, which is used to generate snapshots in the context of the DMDc, forming the foundation upon which the MHE design is based.

5.1 Simulation results for DMDc

The DMDc procedure is implemented in MATLAB using the `svd` function with respect to (11) and it is configured with a truncation order of $p = 10$, making use of data from a total of $m = 200$ snapshots obtained from the parameterized model. The results of the simulation are shown in Fig. 5 and demonstrate a high level of agreement with the parameterized model, thus reflecting excellent consistency with the measured data. The NC error is computed by evaluating the percentage of the absolute difference between the identified model and the DMDc-based model in relation to the maximum value of $N_{\text{Model}}(t)$ such that

$$\Delta N(t) = \frac{|N_{\text{Model}}(t) - N_{\text{DMDC}}(t)|}{\max(N_{\text{Model}}(t))} \times 100, \quad (16)$$

see Fig. 5d. The eigenvalues of the system matrix are situated within the unit circle and represent the detectable modes of (12) for $p = 10$, as shown in Fig. 5e and the reconstructed PSD is depicted in Fig. 5f.

5.2 Simulation results for DMDc-based MHE

The MHE is implemented using a `SQP` algorithm. The estimation time window spans 5 discretization steps corresponding to $\theta = 4.5$ minutes. The MHE approach demonstrates the ability to accurately track measurements, and it exhibits rapid convergence of the estimation error, even in the presence of additive noise on [AZO]. The initial state, represented as $[[Zn]_0, n_0(x)]^T$, is deliberately set to differ from the initially measured states. Refer to Fig. 6 for visual representation and validation of these results. In both Fig. 6b and Fig. 6d the red error dots illustrate the discrepancy

a) AZO mass concentration. b) [AZO](t) error.

c) Number concentration. d) $N(t)$ error.

e) Eigenvalues of $\bar{\mathbf{A}}$ for $p = 10$. f) Reconstructed PSD.
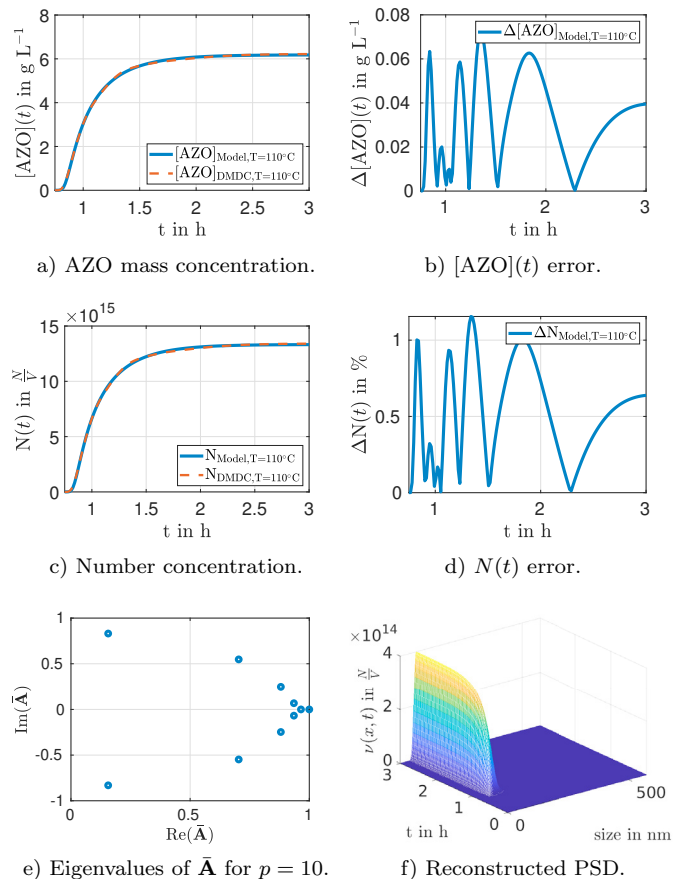
Fig. 5. DMDc simulation results.

between the predicted state and the actual data. The blue error curves depict the difference between estimate and the parameterized model under uncertainties. The reconstructed PSD (continuous colored lines) at sampling times is shown in Fig. 6e. A MHE-iteration step has an average computational time of 0.08s considering an `Intel Core i5-8265U CPU`.

6. CONCLUSIONS

In this study, an early-lumping MHE approach is introduced for the real-time estimation in particulate systems. To achieve precise estimation, optimization-based parameter identification techniques are applied to accurately determine the system's parameters. DMDc is applied, enabling us to derive a linear approximation of the nonlinear system. This discrete linear model forms the core of the MHE, which operates by solving a constrained optimization problem. This optimization problem is tailored to facilitate accurate real-time estimation of the system's state and behavior. As a practical demonstration of the approach, the synthesis of AZO particles is investigated. Our primary objective has been to reconstruct the PSD based on the estimated concentration of AZO nanocrystals. The results showcase the effectiveness and applicability of the approach in providing precise and real-time estimation for our system. This methodology and the obtained results will serve as basis for future research aimed at exploring the control of particle size evolution, along with investi-
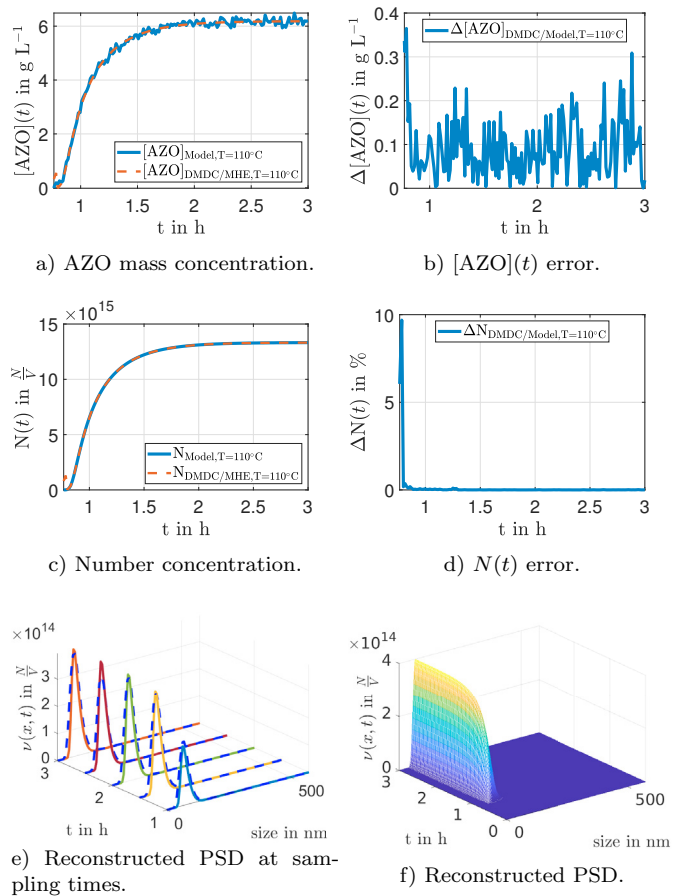
a) AZO mass concentration.

b) $[AZO](t)$ error.

c) Number concentration.

d) $N(t)$ error.

e) Reconstructed PSD at sampling times.

f) Reconstructed PSD.

Fig. 6. DMDc-based MHE simulation results.

gating the size-dependent optical, electrical and thermal properties of the nanocrystals.

REFERENCES

Dongmo, M.K.J. and Meurer, T. (2022). Moving horizon estimator design for a nonlinear diffusion-reaction system with sensor dynamics. *IFAC-PapersOnLine*, 55(20), 85–90. doi:10.1016/j.ifacol.2022.09.076.

Falola, A., Borissova, A., and Wang, X.Z. (2013). Extended method of moment for general population balance models including size dependent growth rate, aggregation and breakage kernels. *Computers & Chemical Engineering*, 56, 1–11. doi: https://doi.org/10.1016/j.compchemeng.2013.04.017.

Garnweitner, G. and Grote, C. (2009). In situ investigation of molecular kinetics and particle formation of water-dispersible titania nanocrystals. *Physical Chemistry Chemical Physics*, 11(19), 3767–3774.

Goertz, V., Gutsche, A., Dingenouts, N., and Nirschl, H. (2012). Small-angle x-ray scattering study of the formation of colloidal sio2 stober multiplets. *The Journal of Physical Chemistry C*, 116(51), 26938–26946.

J. McCoy, B. and Madras, G. (2003). Analytical solution for a population balance equation with aggregation and fragmentation. *Chemical Engineering Science*, 58(13), 3049–3051. doi:10.1016/S0009-2509(03)00159-3.

Kang, Y.S., Ward, J.D., and Nagy, Z.K. (2022). A new framework and a hybrid method for one-dimensional population balance modeling of batch thermocycling

crystallization. *Computers & Chemical Engineering*, 157, 107588. doi:10.1016/j.compchemeng.2021.107588.

Kumar, S. and Ramkrishna, D. (1996). On the solution of population balance equations by discretization—II. a moving pivot technique. *Chemical Engineering Science*, 51(8), 1333–1342. doi:10.1016/0009-2509(95)00355-X.

Kühl, P., Diehl, M., Kraus, T., Schlöder, J.P., and Bock, H.G. (2011). A Real-Time Algorithm for Moving Horizon State and Parameter Estimation. *Computers & Chemical Engineering*, 35(1), 71–83. doi: 10.1016/j.compchemeng.2010.07.012.

Li, X., Bo, S., Zhang, X., Qin, Y., and Yin, X. (2023). Data-driven parallel koopman subsystem modeling and distributed moving horizon state estimation for large-scale nonlinear processes. *AIChE Journal*, e18326.

Nirschl, H. and Guo, X. (2018). Characterisation of structured and functionalised particles by small-angle x-ray scattering (saxs). *Chemical Engineering Research and Design*, 136, 431–446.

Perala, S.R.K. and Kumar, S. (2014). On the two-step mechanism for synthesis of transition-metal nanoparticles. *Langmuir*, 30(42), 12703–12711. doi: 10.1021/la503199m.

Proctor, J.L., Brunton, S.L., and Kutz, J.N. (2016). Dynamic mode decomposition with control. *SIAM Journal on Applied Dynamical Systems*, 15(1), 142–161. doi: 10.1137/15M1013857.

Ramkrishna, D. (2000). *Population balances: theory and applications to particulate systems in engineering*. Academic Press.

Rao, C., Rawlings, J., and Mayne, D. (2003). Constrained State Estimation for Nonlinear Discrete-Time Systems: Stability and Moving Horizon Approximations. *IEEE Trans. Automat. Contr.*, 48(2), 246–258. doi:10.1109/TAC.2002.808470.

Stolzenburg, P. and Garnweitner, G. (2017). Experimental and numerical insights into the formation of zirconia nanoparticles: a population balance model for the non-aqueous synthesis. *Reaction Chemistry & Engineering*, 2(3), 337–348. doi:10.1039/C7RE00005G.

Ungerer, J., Thurm, A.K., Garnweitner, G., and Nirschl, H. (2020a). Evaluation of the dispersion stability of AZO mesocrystals for their processing into functional thin films using small angle x-ray scattering. *Crystals*, 10(5), 374. doi:10.3390/cryst10050374.

Ungerer, J., Thurm, A.K., Garnweitner, G., and Nirschl, H. (2020b). Formation of aluminum-doped zinc oxide nanocrystals via the benzylamine route at low reaction kinetics. *Chemical Engineering & Technology*, 43(5), 797–803. doi:10.1002/ceat.201900466.

Ungerer, J., Thurm, A.K., Meier, M., Klinge, M., Garnweitner, G., and Nirschl, H. (2019). Development of a growth model for aluminum-doped zinc oxide nanocrystal synthesis via the benzylamine route. *Journal of Nanoparticle Research*, 21(5), 106. doi:10.1007/s11051-019-4547-9.

Wu, S. and Yang, W. (2019). Comparisons of methods for reconstructing particle size distribution from its moments. *Fuel*, 252, 325–338. doi: 10.1016/j.fuel.2019.04.124.